Computational Materials Science 167 (2019) 257–263

Contents lists available at ScienceDirect

Computational Materials Science

journal homepage: www.elsevier.com/locate/commatsci

Calculation of the anisotropic coefficients of thermal expansion: A first-principles approach

Nicholas A. Pike[a,*], Ole M. Løvvik[a,b]

[a] Centre for Materials Science and Nanotechnology, University of Oslo, NO-0349 Oslo, Norway
[b] SINTEF Materials Physics, Forskningsveien 1, NO-0314 Oslo, Norway

ARTICLE INFO

Keywords:
Density functional theory
Thermal expansion
Heat capacity

ABSTRACT

Predictions of the anisotropic coefficients of thermal expansion are needed to not only compare to experimental measurement, but also as input for macroscopic modeling of devices which operate over a large temperature range. While most current methods are limited to isotropic systems within the quasiharmonic approximation, our method uses first-principles calculations and includes anharmonic effects to determine the temperature-dependent properties of materials. These include the lattice parameters, anisotropic coefficients of thermal expansion, isotherm bulk modulus, and specific heat at constant pressure. Our method has been tested on two compounds (Cu and AlN) and predicts thermal properties which compare favorably to experimental measurement over a wide temperature range.

1. Introduction

While experimental measurements of the coefficient of thermal expansion (CTE) can be done using a number of experimental techniques [1–5], most theoretical tools available for predicting the CTE are limited to the quasiharmonic approximation (QHA) or the Debye-Gruneisen approximation. There are a few programs [6,7] and several models [8–22] available for scientists to calculate the CTE, and its associated thermal properties, from first-principles calculations. These currently available methods principally rely on the QHA. Since these programs determine the coefficient of volume expansion, they are limited to calculations of systems with a considerable amount of structural symmetry. A limited amount of work has been published on the thermal properties of anisotropic systems employing anharmonic effects [23–25], but this work is not available as a comprehensive package of tools that can automatically predict such properties from a first-principles approach.

In this work, an algorithm is developed to determine the thermal properties of isotropic and anisotropic systems using density functional theory (DFT) and density functional perturbation theory (DFPT) calculations. This algorithm utilizes the Vienna Ab initio Simulation Package (VASP) [26–28] for first-principles calculations and the temperature-dependent effective potential (TDEP) [29–31] software package to calculate the interatomic force constants. The TDEP method is designed to work for both harmonic and strongly anharmonic systems [31].

To demonstrate the abilities of our methods, two systems with distinctive symmetries are compared to a variety of experimental results. The first system, pure copper (Cu) [35,36], possesses cubic symmetry and therefore the CTE is a single temperature-dependent value. The temperature-dependent properties of copper are thoroughly investigated experimentally [33,35,37–44] and Cu is consequently used to determine the quality of our calculation methods. The second material, aluminum nitride (AlN) [34], is widely used in electronic devices applications and has a hexagonal crystal structure. Therefore, AlN has two unique CTE's and is used to demonstrate our ability to calculate the expansion coefficients of an anisotropic material with a known temperature-dependent anharmonic interaction [23]. In each case, our algorithm outputs a large amount of temperature dependent information that can be used to better understand thermal expansion in macroscopic devices by modeling interfaces at finite temperatures which, when there are differences in the thermal expansion rates across the interfaces, can lead to mechanical failure during thermal cycling.

In Section 2, an outline of the calculation methods is provided and in Section 3, we analyze the results of our methods via comparison to available experimental data for Cu and AlN. Finally, in Section 4, we provide a concluding discussion.

2. Calculation methods

The present benchmark calculations were performed with the

* Corresponding author.
E-mail address: Nicholas.pike@smn.uio.no (N.A. Pike).

https://doi.org/10.1016/j.commatsci.2019.05.045
Received 15 March 2019; Received in revised form 20 May 2019; Accepted 21 May 2019
0927-0256/ © 2019 The Author(s). Published by Elsevier B.V. This is an open access article under the CC BY-NC-ND license (http://creativecommons.org/licenses/BY-NC-ND/4.0/).

projector-augmented wave (PAW) method [45] to describe the core electrons by utilizing PAW pseudopotentials [46]. Exchange and correlations effects were described by the Perdew-Burke-Ernzerhof (PBE) generalized gradient approximation (GGA) [47]. To describe the electronic system, a plane-wave energy cutoff equal to 500 eV was used and a Monkhorst-Pack [48] mesh of points was generated for each grid in reciprocal space assuming a k-point density of at least five points per $Å^{-1}$. For the relaxation, ground-state, and configuration calculations the same k-point mesh was used. DFPT calculations were done on a k-point mesh twice as dense as the grid used in the ground state calculations.

For each ground state and configuration calculation, the iterations of the total energy were stopped once the differences in energy between successive iterations were less than 0.01 meV per unit cell. To calculate the dielectric, elastic, and Born effective charge of our material, we used finite-differences as implemented within VASP where only symmetry-inequivalent atomic displacements were used to calculate the Hessian matrix. The elastic tensor was used to determine the Debye temperature and the isentropic bulk modulus, as outlined below. The dielectric tensor and Born effective charge tensor were used to account for the long-range electrostatic interactions in semiconducting compounds within TDEP.

Using DFT and DFPT, the elastic tensor is first calculated allowing us to calculate various moduli, speeds of sound, and the Debye temperature as follows. First, the Voigt average of the bulk (B) and shear (G) moduli (upper bound for polycrystalline materials) are found from the components of the elastic tensor, C_{ij} ($i, j = 1. .6$), as [49,50]

$$\begin{aligned} B &= \tfrac{1}{9}((C_{11} + C_{22} + C_{33}) + 2(C_{12} + C_{31} + C_{23})) \\ G &= \tfrac{1}{15}((C_{11} + C_{22} + C_{33}) - (C_{12} + C_{31} + C_{23}) \\ &\quad + 3(C_{44} + C_{55} + C_{66}). \end{aligned} \tag{1}$$

With the bulk and shear moduli one can then calculate the longitudinal and shear sound velocities (v_l and v_s) as [51]

$$v_l = \sqrt{\frac{B + 4/3G}{\rho}} \tag{2}$$

and

$$v_s = \sqrt{\frac{G}{\rho}}, \tag{3}$$

where ρ is the density of the material. Therefore, the Debye temperature can be calculated as [51]

$$\Theta_D = \frac{h}{k_B}\left[\frac{9m}{4\pi}\right]^{1/3}\left[\left(\frac{1}{v_l^3} + \frac{2}{v_s^3}\right)\right]^{-1/3}, \tag{4}$$

where h is Planck's constant, k_B is the Boltzmann constant, and m is the number of atoms per volume. Unlike in Ref. [51], we do not separate the acoustic bands and use all the phonon bands to calculate θ_D.

Since θ_D is calculated from the elastic tensor, which is calculated at zero temperature within VASP, it also represents the ground state (0 K) θ_D. While one could, in principle, calculate the elastic properties as a function of temperature [57,22], and therefore θ_D as a function of temperature, we have found that the value of θ_D at zero temperature provides an adequate starting point for our calculations since variations in the configuration temperature, outlined below, do not significantly modify our results.

θ_D is used within TDEP to generate an initial guess for the force constants of the system. They are in turn employed to generate atomic configurations based on a canonical ensemble. Here, twelve configurations are generated as follows: with θ_D and the symmetry of the cell, one generates an initial guess for the interatomic force constants and solves the equations of motion for the system by finding the resulting eigenvalues and eigenvectors. Then, these eigenvalues and eigenvectors are used to determine the amplitude and velocity of each atom chosen such that these quantities are normally distributed over a canonical ensemble. The configurations consisted in this study of 208 atoms for Cu and AlN. The ensemble is generated at a finite temperature (here designated the configuration temperature) with Bose-Einstein statistics used to determine the mean normal mode amplitude [58]. VASP is then used to calculate the energies, displacements, and forces for each of the generated configurations. These are combined within TDEP to generate the finite-temperature force constants by fitting the Born-Oppenheimer energy surface. This procedure allows us to go beyond the quasi-harmonic approximation by explicitly including anharmonic effects through the canonical ensembles.

The extracted force constants are used to find the phonon frequencies and phonon density of states (pDOS) on a q mesh in reciprocal space (in this work $30 \times 30 \times 30$ points were used) using the tetrahedron integration approach [59]. Using this grid and integration method ensured the convergence of the free energy to within 0.01 meV/atom.

The calculated lattice parameters $\mathbf{x}(T, p)$ depend on temperature and pressure. Determining the lattice parameters at ambient pressure $\mathbf{x}(T, 0)$ requires minimizing the free energy $F(\mathbf{x}, T)$ at each temperature. The free energy of the system can be expressed as a function of the total electronic energy $U(\mathbf{x})$ and the vibrational free energy ($F_{\text{vib}}(\mathbf{x}, T)$) as

$$\begin{aligned} F(\mathbf{x}, T) &= U(\mathbf{x}) + F_{\text{vib}}(\mathbf{x}, T), F_{\text{vib}}(\mathbf{x}, T) \\ &= \int_0^{\omega_{max}} \sum_\lambda \left[g(\omega_\lambda)\frac{\hbar\omega_\lambda}{2} + k_B T g(\omega_\lambda) \ln\left(1 - \exp\left(\frac{\hbar\omega_\lambda}{k_B T}\right)\right)\right] d\omega_\lambda, \end{aligned} \tag{5}$$

where λ is the phonon mode index and both the vibrational density of states ($g(\omega)$) and phonon frequencies ω_λ depend on $\mathbf{x}$. U is the DFT calculated volume dependent total electronic energy of the system. In order to minimize $F(\mathbf{x}, T)$, a set of lattice parameters is generated automatically by applying strain to the system around the ground state equilibrium lattice parameters. This is done by finding a series of six lattice parameters in each symmetry unique direction such that the new lattice parameters range between one percent compressive and four percent tensile strain. This provided a smooth free energy surface at each temperature.

The optimized lattice parameters $\mathbf{x}_0(T)$ are found by fitting $F(\mathbf{x}, T)$ to a polynomial function [14,16,25] of the lattice parameters $x_i = a$, b, and c as $F_{\text{fit}}(\mathbf{x}) = \sum_{i,j} f_{i,j,k} a^i b^j c^k$, where $f_{i,j,k}$ are the coefficients of the polynomial fit. Here, we used fourth-order polynomials, and varied a (a and c) in the case of Cu (AlN).

To determine the minimum of $F(\mathbf{x}, T)$, we use the constrained BFGS minimization method as implemented in the Scipy optimize package [60–62]. After finding these minimizing parameters they are fitted to an eighth-order polynomial as a function of temperature to account for the numerical noise in the free energy calculations. The CTE is then calculated by computing the derivative of the smoothed data [55] ($\alpha_{x_i} = \frac{1}{x_i^0}\frac{d\, x_i}{dT} = \frac{d\, \ln(x_i)}{dT}$) for each component of the CTE. x_i^0 is either the zero temperature lattice constant or the temperature-dependent lattice constant, as shown here. Using either of these produces practically identical results, as assumed by Slack [55].

With the integrated pDOS, the specific heat at constant volume (C_v) is calculated for the relaxed geometry and the specific heat at constant pressure (C_p) is found using the well-known thermodynamic relationship

$$C_p = C_v + VT\frac{\text{Tr}(\alpha)^2}{\beta_T}. \tag{6}$$

Here, $\text{Tr}(\alpha)$ is the trace of the CTE matrix and β_T is the isothermal compressibility, which is the inverse of the isothermal bulk modulus B_T. B_T is determined by fitting the free energy at a fixed temperature versus volume using the Birch-Murnaghan equation of state [63–65]. This

allows us to extract the cohesive energy and the pressure derivative of B_T as a function of temperature. There is no significant numerical difference between B_T and the isoentropic bulk modulus B_s in solids [66]; however, the methods used to calculate and measure these quantities are different and thus we distinguish these two quantities whenever possible.

Additional details of our algorithm are presented within the Appendix A.

3. Results

To test the accuracy of our VASP and TDEP calculations and the accuracy of our algorithm, we will compare our calculated values to experimental results for well-known systems: bulk Cu and AlN. Bulk Cu is a face-centered cubic structure (space group $Fm\bar{3}m$) from 0 K to its melting point of approximately 1357 K [67,68]. Bulk AlN has a wurtzite (hexagonal) crystal structure (space group $P6_3mc$) from 0 K to its melting point of approximately 3270 K [69]. For each material, our calculations can be compared to experimental measurement as shown in Table 1.

Table 1 contains a comparison of our ground state (0 K) calculated Debye temperature, isentropic bulk modulus, and DFT lattice parameters to experimental measurement. The agreement between our values and experiment is well within the typical errors seen in ground state GGA-DFT calculations.

The temperature-dependent lattice parameters of Cu and AlN are shown in Fig. 1. They are compared to experimental values. In the case of Cu, the recommended values of the thermal lattice expansion given in Ref. [33] were used as reference. The difference between our calculated values and experimental measurement comes from the inherent error in predicting the ground state lattice parameters at the specific level of theory (i.e.: the PBE GGA of DFT). The calculated lattice parameters were fitted to an eight order polynomial, shown as solid lines. In addition, black dashed lines show the results adjusted for the DFT ground state error for the sake of comparison.

Table 1
Our ground state (0 K) calculated Debye temperature, isentropic bulk modulus, and lattice parameters compared to experimental values. The experimental lattice parameters of Cu and AlN come from experimental data extrapolated to zero temperature.

	Cu			AlN		
	Calc.	Exp.	Ref.	Calc.	Exp.	Ref.
Θ_D (K)	348	347	[70]	1048	971	[71]
B (GPa)	143.8	137.6	[72]	196.5	201	[73]
a (Å)	3.633	3.615	[74]	3.129	3.107	[75]
c (Å)				5.012	4.973	[75]

The unshifted polynomial fit was used to calculate the CTE, specific heat, and bulk modulus. We obtain excellent agreement between the calculated CTE and experimental measurements for Cu and AlN between approximately 30 K and θ_D, as shown in Fig. 2. However, there is some deviation above θ_D, most notably for Cu where the calculated CTE is markedly higher than the experimental values as the temperature approaches the melting temperature. This is most likely due to higher-order anharmonic interactions not sufficiently accounted for at these temperatures. For AlN, it has been shown that the temperature-dependent c/a ratio is not correctly reproduced in anharmonic DFT/TDEP calculations [23], and our extracted anisotropic CTE of AlN are consistent with those results.

The calculated specific heats of these materials also agree very well with experimental measurement as shown in Fig. 3. We also calculated C_p for both materials, but the difference between C_v and C_p was too small over the entire temperature range of data to be discernible in the plot—at any temperature the difference $1 - (C_p/C_v)$ was smaller than 10^{-6}. This calculation, therefore, is further evidence that one can safely ignore the differences between these two quantities when comparing experimental and theoretical values [78].

Finally, in Fig. 4, we plot B_T and its pressure derivative vs temperature for both Cu and AlN. Literature values of B_T and B_s are shown for the sake of comparison. B_s lies consistently above both theoretical and experimental values of B_T, most likely due to error in finding the experimental values of the elastic constants.

4. Discussion and conclusion

Our algorithm calculates the thermal expansion of both isotropic and anisotropic materials using the DFT, DFPT and TDEP methods. Several related thermal properties are also calculated including B_T and C_p. Agreement between our calculations and experimental results gives us confidence in our methods. The correspondence between our calculations and experiment for the CTE is only moderate at temperatures above θ_D. This may e.g. be due to unattributed numerical inaccuracies,

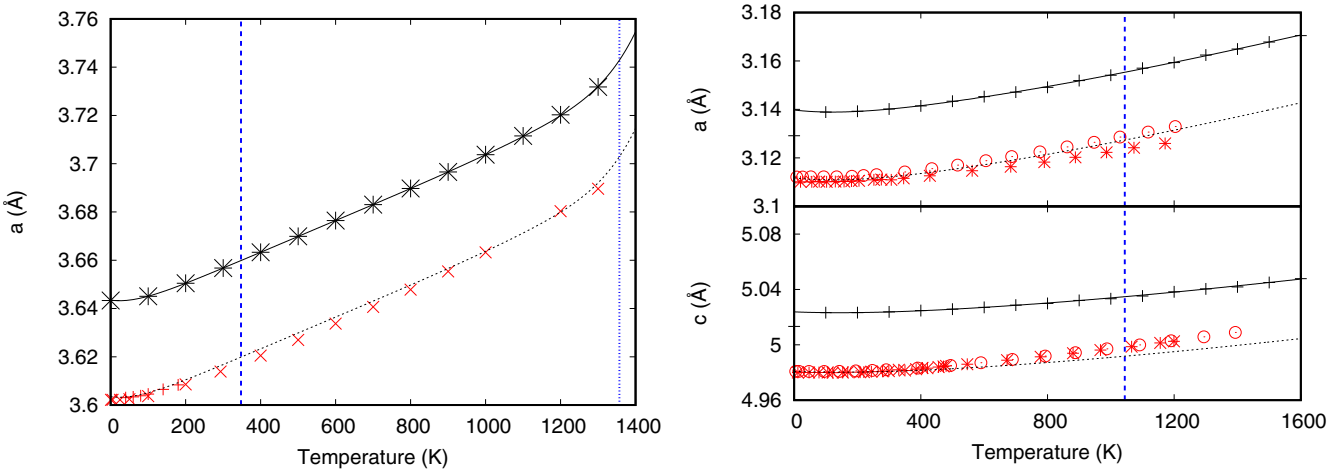

Fig. 1. Calculated and experimental temperature-dependent lattice parameters for Cu (left panel) and AlN (right panel). Our calculations are shown as black points (every 50th point is shown) and the solid line corresponds to an eighth order polynomial fit. The black dashed line equals the solid line except for a constant shift correcting for the ground state error originating from the PBE GGA calculations. Data, in red, for Cu from Ref. [32] (+) and the recommended lattice parameter of Ref. [33] (X). Data for AlN from Refs. [34] (∗) and [17] (⊙). Here and in all the following figures, the blue dashed and dotted vertical lines denote the Debye and melting temperature respectively. (For interpretation of the references to colour in this figure legend, the reader is referred to the web version of this article.)

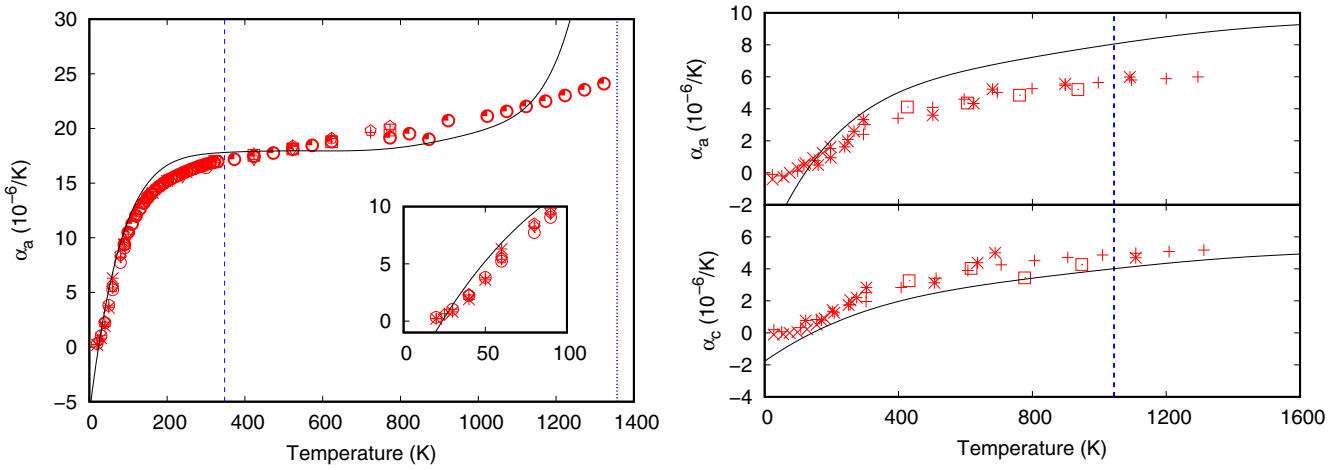

Fig. 2. The CTE for Cu (left panel) and AlN (right panel) from our calculations as a solid line and experimental data as red symbols. For Cu, + (Ref. [35]), × (Ref. [37]), ∗ (Ref.[38]), (Ref. [40]), ⊙ (Ref. [41]), ▽ (Ref. [42]), ◇ (Ref. [43]), ⬠ (Ref. [52]) and quarter open circles (Ref. [53]). For AlN, + (Ref. [17]), × (Ref. [54]), ∗ (Ref. [55]), and (Ref. [56]). Inset: Calculated and experimental data points for temperatures between 0 and 100 K indicating that our calculations are only accurate for $T > 30$ K.

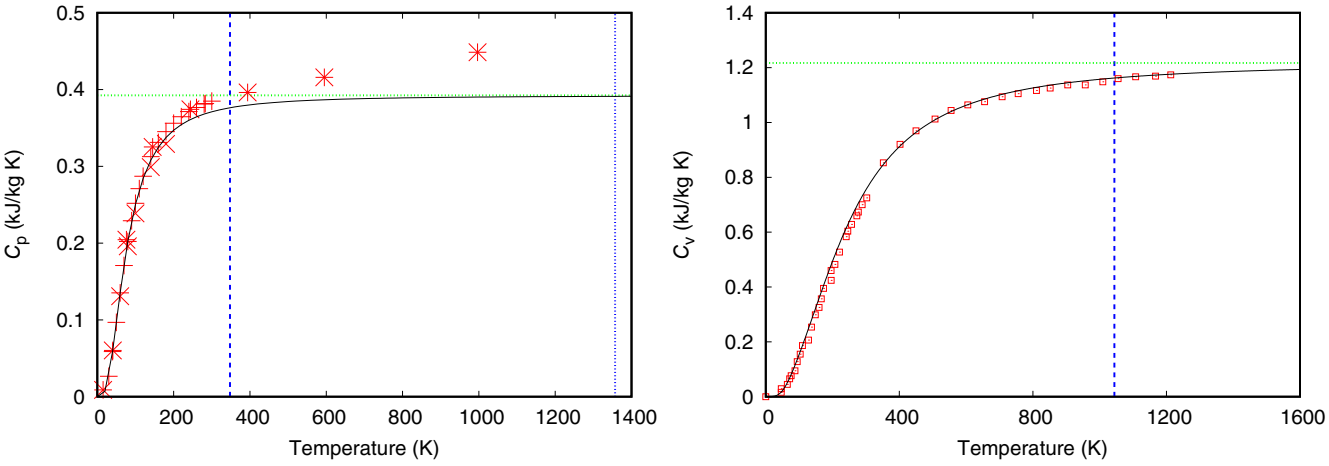

Fig. 3. Calculated C_p for Cu (left panel) and C_v for AlN (right panel) as solid lines. The corresponding literature data is given as red points. For Cu, + from Ref. [36], × from Ref. [32], and ∗ from Ref. [76]. For AlN, the data comes from Ref. [77]. The green dashed line in both panels is the Dulong-Petit limit. (For interpretation of the references to colour in this figure legend, the reader is referred to the web version of this article.)

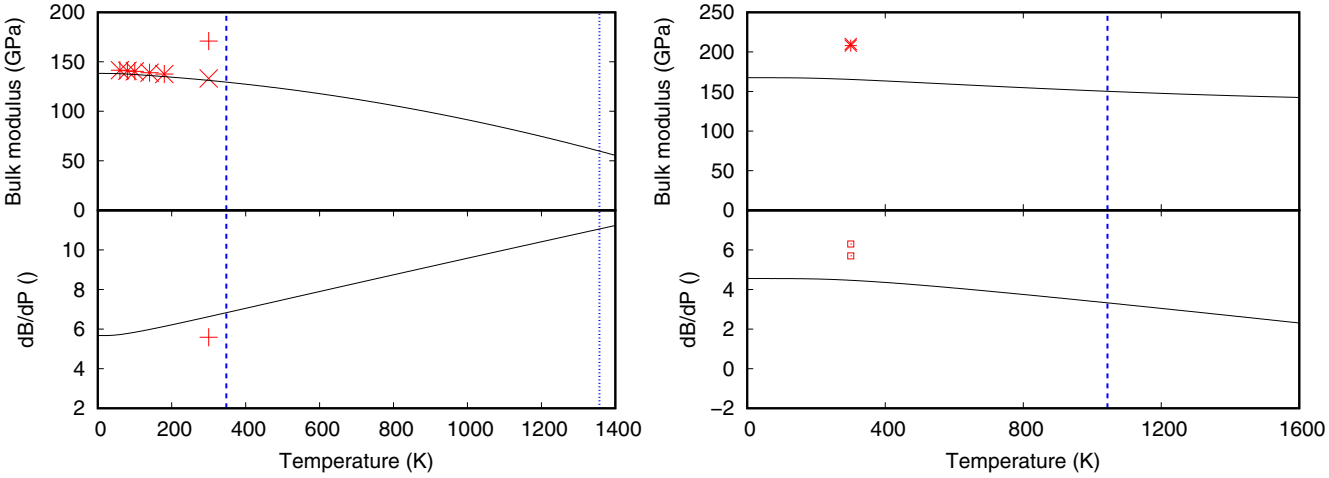

Fig. 4. Calculated isothermal bulk modulus (upper panels), and its pressure derivative (lower panels), for Cu (left panels) and AlN (right panels) as solid lines. Data points in red. For the upper left panel: + (Ref. [79]) for the isoentropic bulk modulus, ×(Ref. [80]), and ∗ (Ref. [32]) are for the isothermal bulk modulus. For the lower left panel: + (Ref. [79]) using the isoentropic bulk modulus. Upper right panel: × (Ref. [81]), and + (Ref. [82]). Lower right panel: (Ref. [83]). (For interpretation of the references to colour in this figure legend, the reader is referred to the web version of this article.)

the present level of theory (PBE-GGA), or due to an inadequate sampling of the anharmonic interactions at elevated temperatures due to the finite number of configurations used in this calculation. Nevertheless, most of our predictions are very well aligned with experiment, which makes us confident that this software can be used to determine the CTE for many more materials of experimental interest either with individual calculations or as part of a high-throughput framework.

We have undertaken several careful convergence studies of the number of configurations, super-cell size, and k-point mesh density to minimize the error between our calculations and experimental measurement over the entire temperature range. We have determined that using the k-point mesh density given previously provides a reasonable accuracy between our calculated CTE and experiment. Additionally, we have found that the configuration temperature used by TDEP should be slightly smaller than θ_D allowing for us to account for most of the anharmonic interactions as the temperature approaches the melting temperature. Here, we show results with the configuration temperature equal to 80% of θ_D and have tested both higher and lower configuration temperatures as well with similar results.

While not shown, the present algorithm can be used to calculate the CTE from a completely anisotropic system. Additionally, this algorithm can easily be integrated into existing high-throughput software workflows that we hope will enable subsequent researchers in e.g. designing the next generation temperature-dependent electronics. While one must use caution when calculating temperature-dependent properties, and carefully consider the convergence of many of the DFT, DFPT, and TDEP input parameters, this software thus provides an algorithm for automatically calculating the CTE and related properties of any material with a periodic unit cell. The symmetry and size of this unit cell may be limiting factors of the choice of materials, since it may be prohibitively expensive to perform calculations on very large unit cells with low symmetry with currently available high performance computing resources.

Data availability

The raw and processed data required to reproduce these findings are available to download fromhttps://GitHub.com/Npikeulg/ACTE.

Acknowledgments

We would like to thank the Research Council of Norway through the Frinatek program for funding and Martin Fleissner Sunding, Olle Hellman, and Nina Shulumba for helpful conversations and support. The computations were performed on resources provided by UNINETT Sigma2 – the National Infrastructure for High-Performance Computing and Data Storage in Norway through Grant Nos. nn2615k and nn9462k.

Appendix A. Summary of the algorithm

Our algorithm for calculating the CTE and associated thermal properties is diagrammed in Fig. 5 which involves both serial and parallel computations using VASP and TDEP. To start a calculation, the user enters a single VASP formatted POSCAR file describing the material's crystal structure into the directory where the entire calculation will take place. This POSCAR file should represent the conventional cell of the system in the desired symmetry and, preferably, should represent the DFT-relaxed ground state structure. To launch the calculations, the user should execute the script with the tag "–relaxation" which generates the necessary input files and bash scripts, creates the directories for the VASP calculations, and checks the

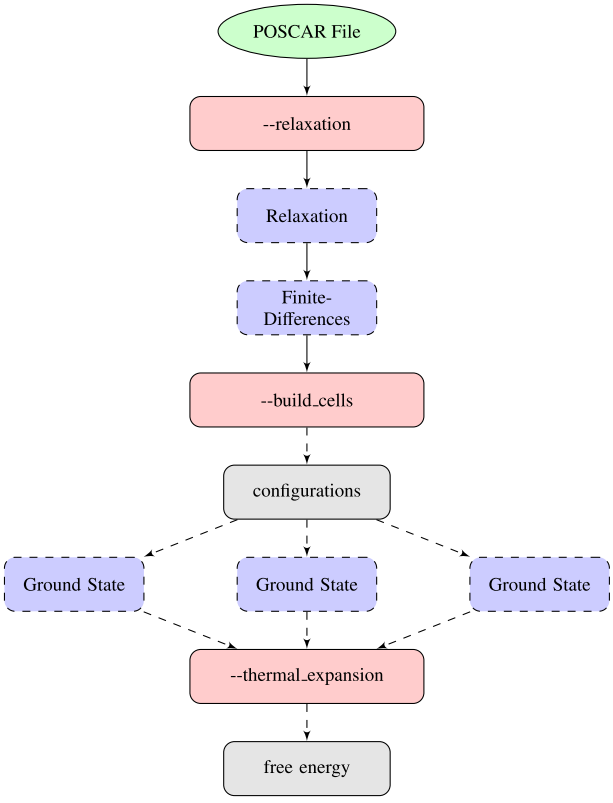

Fig. 5. Flow-chart outlining the algorithm used to calculate the anisotropic CTE. Blue rectangles represent first-principles calculations using VASP and red rectangles represent calculations done with our script. TDEP calculations (gray rectangles) are automatically launched by our script during the last two stages of the calculation. Solid rectangles and lines correspond to serial calculations and dashed lines and rectangles represent parallel calculations.

convergence of the calculations once completed. Following a relaxation calculation to ensure convergence, the script will automatically launch the finite-differences calculations for the needed tensor quantities. Should the algorithm detect an error in the data or convergence procedure, the code will abort. Once the error is fixed, the user can relaunch the calculation.

After the finite-differences calculation, our algorithm automatically starts the next stage of the calculation (which can be manually executed with –build_cells) that constructs a set of unit cells corresponding to different volumes. The algorithm generates the necessary lattice parameter perturbations, as described above, to determine the CTE for the compound. During this calculation, the script will analyze the symmetry of the relaxed unit cell, calculate the Debye temperature for the creation of the initial set of configurations used by TDEP to determine the inter-atomic force constants, and generate the necessary files for the related VASP calculations. Once generated, the algorithm will rerun the relaxation of the newly perturbed unit cell by allowing relaxation of only the atomic positions. After this second relaxation, the script will generate the configurations and launch each configuration in parallel. Since this is the most time-consuming part of the calculation, the user can relaunch this calculation as needed and only the parts of the calculation that are incomplete will be executed.

The finishing stage of this calculation can be executed with the tag "–thermal_expansion" in which the script, for each lattice perturbation, will launch TDEP to post-process the results of the previous VASP calculations. This post-processing generates the phonon density of states and various thermal properties including the free energy of the system. After gathering the calculated free energies, the script will determine the set of lattice parameters that minimize the free energy as a function of temperature. This temperature dependent set of lattice parameters is used to determine the CTE, isothermal bulk modulus, and specific heat at constant pressure as outlined above.

During the concluding stage of the calculation, several output files are produced. The calculated free energies for each volume as a function of temperature are printed to a single data file "out.free_energy_vs_temp" with temperatures given in Kelvin and free energies given in eV. The temperature dependent lattice parameters are printed to a file called "out.thermal_expansion" with the lattice parameters given in Å. The thermal expansion coefficients are printed to the file "out.expansion_coeffs" in units of K^{-1}. Calculations of the isothermal bulk modulus, its pressure derivative, and cohesive energy are printed to the file "out.isothermal_bulk" where the isothermal bulk modulus is given in GPa, the derivative of the bulk modulus with respect to pressure is unit-less, and the cohesive energy is in eV. Finally, the specific heat at constant volume and constant pressure are calculated. These are printed to the data file "out.cv_cp" where both specific heats are given in units of $kJ\,kg^{-1}\,K^{-1}$.

References

[1] R.I. Belousov, S.K. Filatov, Algorithm for calculating the thermal expansion tensor and constructing the thermal expansion diagram for crystals, Glass Phys. Chem. 33 (2007) 271–275.
[2] M.J. Cliffe, A.L. Goodwin, Pascal: a principle axis strain calculator for thermal expansion and compressibility determination, J. Appl. Cryst. 45 (2012) 1321–1329.
[3] Z.A. Jones, P. Sarin, R.P. Haggerty, W.M. Kriven, Cteas: a graphical-user-interface-based program to determine thermal expansion from high-temperature x-ray diffraction, J. Appl. Cryst. 46 (2013) 550–553.
[4] S.G. Samovilov, A.I. Orlova, G.N. Kazantsev, A.V. Bankrashkov, A technique for determing thermal expansion coefficients in cubic, tetragonal, hexagonal, and orthorhombic crystals, Crystal. Repts. 51 (2006) 486–489.
[5] C. Dudescu, J. Naumann, M. Stockmann, S. Nebel, Characterizsation of thermal expansion coefficient of anisotropic materials by electronic speckle pattern interferometry, Strain 42 (2006) 197–205.
[6] A. Togo, I. Tanaka, First principles phonon calculations in materials science, Scr. Mater. 108 (2015) 1–5.
[7] A. Togo, L. Chaput, I. Tanaka, G. Hug, First-principles phonon calculations of thermal expansion in Ti_3SiC_2, Ti_3AlC_2, and Ti_3GeC_2, Phys. Rev. B 81 (2010) 174301.
[8] A.I. Lichtenstein, R.O. Jones, S. de Gironcoli, S. Baroni, Anisotropic thermal expansion in silicates: a density functional study of β-eucryptite and related materials, Phys. Rev. B 62 (2000) 11487.
[9] L. He, F. Liu, G. Hautier, M.J.T. Oliveria, M.A.L. Marques, F.D. Vila, J.J. Rehr, G.-M. Rignanese, A. Zhou, Accuracy of generalized gradient approximation functionals for density-functional perturbation theory calculations, Phys. Rev. B 89 (2014) 064305.
[10] P. Carrier, R. Wentzcovitch, J. Tsuchiya, First-principles prediction of crystal structures at high temperature using the quasiharmonic approximation, Phys. Rev. B 76 (2007) 064116.
[11] A. Fleszar, X. Gonze, First-principles thermodynamical properties of semiconductors, Phys. Rev. Lett. 64 (1990) 2961.
[12] H.M. Jin, P. Wu, First principles calculation of thermal expansion coefficient: part 1: cubic metals, J. Alloys Compd. 343 (2002) 71–76.
[13] A.A. Quong, A.Y. Liu, First-principles calculations of the thermal expansion of metals, Phys. Rev. B 56 (1997) 7767.
[14] T. Tohei, Y. Wananabe, H.-S. Lee, Y. Ikuhara, First principles calculation of thermal expansion coefficients of pure and Cr doped α– alumina crystals, J. Appl. Phys. 120 (2016) 142106.
[15] G. Liu, J. Zhou, H. Wang, Anisotropic thermal expansion of snse from first-principles calculations based on gruneisen's theory, Phys. Chem. Chem. Phys. 19 (2017) 15187–15193.
[16] S.Q. Wang, First-principles study of the anisotropic thermal expansion of wurtzite ZnS, Appl. Phys. Lett. 88 (2006) 061902.
[17] K. Wang, R.R. Reeber, Thermal expansion of GaN and AlN, MRS Proc. 482 (2011) 863.
[18] Y. Ding, B. Xiao, Thermal expansion tensors, gruneisen parameters and phonon velocities of bulk mt_2 (m = mo, w, t = s and se) from first principles calculations, RSC Adv. 5 (2015) 18391.
[19] S. Lamowski, S. Schmerler, J. Kutzner, J. Kortus, First principles calculations of the thermal volume expansion coefficient of tetragonal zircon dioxide, Steel Res. Int. 82 (2011) 1129–1132.
[20] G. Liu, J. Zhou, First-principles study of thermal expansion and thermomechanics of group-v monolayers: blue phosphorene, arsenene, adn antimonene, J. Phys.: Condens. Matter 31 (2018) 065302.
[21] S.D. Gilev, Few-parameter equation of state of copper, Combust. Explosion Shock Wave 54 (2018) 482–495.
[22] G.-M. Rignanese, J.-P. Michenaud, X. Gonze, Ab initio study of the volume dependence of dynamical and thermodynamical properties of silicon, Phys. Rev. B 53 (1996) 4488.
[23] N. Shulumba, Z. Raza, O. Hellman, E. Janzen, I.A. Abrikosov, M. Oden, Impact of anharmonic effects on the phase stability, thermal transport, and electronic properties of aln, Phys. Rev. B 94 (2016) 104305.
[24] N. Shulumba, O. Hellman, L. Rogstrom, Z. Raza, F. Tasnadi, I.A. Abrikosov, M. Oden, Temperature-dependent elastic properties of $Ti_{1-x}Al_xN$ alloys, Appl. Phys. Lett. 107 (2015) 231901.
[25] S. Schmerler, J. Kortus, Ab initio study of aln: anisotropic thermal expansion, phase diagram, and high-temperature rocksalt to wurtzite phase transition, Phys. Rev. B 89 (2014) 064109.
[26] G. Kresse, J. Hafner, Ab initio molecular dynamics for open-shell transition metals, Phys. Rev. B 48 (1993) 13115.
[27] G. Kresse, J. Furthmuller, Efficiency of ab-initio total energy calculations for metals and semiconductors using a plane-wave basis set, Comput. Mater. Sci. 6 (1996) 15.
[28] G. Kresse, J. Furthmuller, Efficient iterative schemes for ab initio total-energy calculations using a plane-wave basis set, Phys. Rev. B 54 (1996) 11169.
[29] O. Hellman, I.A. Abrikosov, Temperature-dependent effective third-order interatomic force constants from first-principles, Phys. Rev. B 88 (2013) 144301.
[30] O. Hellman, P. Steneteg, I.A. Abriksov, S.I. Simak, Temperature dependent effective potential method for accurate free energy calculations of solids, Phys. Rev. B 87 (2013) 104111.
[31] O. Hellman, I.A. Abrikosov, S.I. Simak, Lattice dynamics of anharmonic solids from first-principles, Phys. Rev. B 84 (2011) 180301.
[32] J.S. Shah, Thermal Lattice Expansion of Various Types of Solids (Ph.D. thesis), University of Missouri-Rolla, 1944.
[33] Y.S. Touloukian, R.K. Kirby, R.E. Taylor, P.D. Desai, Thermophysical Properties of Matter– The TPRC Data Series– Vol. 12. Thermal Expansion Metallic Elements and Alloys (Technical Report), Purdue University, 1975.
[34] S. Figge, H. Kroncke, D. Hommel, B.M. Epelbaum, Temperature dependence of the thermal expansion of aln, Appl. Phys. Lett. 94 (2009) 101915.
[35] T.A. Hahn, Thermal expansion of copper from 20 to 800k- standard reference material 736, J. Appl. Phys. 41 (1970) 5096.
[36] G.K. White, Thermal expansion of reference materials: copper, silica, and silicon, J. Phys. D: Appl. Phys. 6 (1973) 2070.
[37] H. Adenstedt, Studien zur thermischen ausdehnung fester stoffe in tiefer temperatur (Cu, Ni, Fe, Zinkblende, LiF, Kalkspat, Aragonit, NH_4Cl), Ann. Phys. 26 (1936) 65.
[38] R.H. Carr, R.D. McCammon, G.K. White, The thermal expansion of copper at low temperatures, Proc. Roy. Soc. London: A Math. Phys. Sci. 280 (1964) 72–84.
[39] R.H. Carr, C.A. Swenson, Application of a variable transformer to the study of low temperature thermal expansion, Cryogenics 4 (1964) 76–82.
[40] H. Esser, H. Eusterbrock, Untersuchung der wrmeausdehnung von einigen metallen und legierungen mit einem verbesserten dilatometer, Arch. Eisenhuttenw. 14 (1941) 341.
[41] D.B. Fraser, A.C.H. Hallett, The coefficient of thermal expansion of various cubic metals below 100 k, Can. J. Phys. 43 (1965) 193.

[42] I.I. Lifanov, N.G. Sherstyukov, Thermal expansion of copper in the temperature range -185 to +300c, Thermophys. Meas. 12 (1968) 1653.
[43] T. Rubin, H.W. Altman, H.L. Johnston, Coefficients of thermal expansion of solids at low temperatures. i. the thermal expansion of copper from 15 to 300k, J. Am. Chem. Soc. 76 (1954) 5289–5293.
[44] J.W. Arblaster, Thermodynamic properties of copper, J. Phase Eq. Diff. 36 (2015) 422.
[45] P.E. Blochl, Projector augmented-wave method, Phys. Rev. B 50 (1994) 17953.
[46] G. Kresse, D. Joubert, From ultrasoft pseudopotentials to the projector augmented-wave method, Phys. Rev. 59 (1999) 1758.
[47] J.P. Perdew, K. Burke, M. Ernzerhof, General gradient approximation made simple, Phys. Rev. Lett. 77 (1996) 3865.
[48] H.J. Monkhorst, J.D. Pack, Special points for brillouin zone integrations, Phys. Rev. B 13 (1976) 5188–5192.
[49] J.F. Nye, Physical Properties of Crystals, Oxford University Press, London, 1957.
[50] N.A. Pike, B.V. Troeye, A. Dewandre, X. Gonze, M.J. Verstraete, Vibrational and dielectric properties of the bulk transition metal dichalcogenides, Phys. Rev. Mater. 2 (2018) 063608.
[51] T. Jia, G. Chen, Y. Zhang, Lattice thermal conductivity evaluated using elastic properties, Phys. Rev. B 95 (2017) 155206.
[52] R.O. Simmons, R.W. Balluffi, Measurement of equilibrium concentrations of vacancies in copper, Phys. Rev. 129 (1963) 1533.
[53] I.E. Leksina, S.I. Novikova, Thermal expansion of copper, silver, and gold within a wide range of temperatures, Fiz. Tverd. Tela. 5 (1963) 1094–1099.
[54] N. Ivanov, P.A. Popov, G.V. Egorov, A.A. Sidorov, B.I. Kornev, L.M. Zhukova, V.P. Ryabov, Thermophysical properties of aluminum nitride ceramic, Phys. Solid State 39 (1997) 81–83.
[55] G.A. Slack, S.F. Bartram, Thermal expansion of some diamondlike crystals, J. Appl. Phys. 46 (1975) 89.
[56] W.M. Yim, R.J. Paff, Thermal expansion of AlN, Sapphire, and Silicon, J. Appl. Phys. 45 (1974) 1456.
[57] P. Steneteg, O. Hellman, O.Y. Vekilova, N. Shulumba, F. Tasnadi, I.A. Abrikosov, Temperature dependence of tin elastic constants from ab initio molecular dynamic simulations, Phys. Rev. B 87 (2013) 094114.
[58] D. West, S.K. Estreicher, First-principles calculations of vibrational lifetimes and decay channels: hydrogen-related modes inSi, Phys. Rev. Lett. 96 (2006) 115504.
[59] G. Lehmann, M. Taut, On the numerical calculation of the density of states and related properties, Phys. Status Solidi B 54 (1972) 469.
[60] E. Jones, T. Oliphant, P. Peterson, et al., Scipy: open source scientific tools for python, 2001.http://www.scipy.org/ (accessed: 30.10.2018).
[61] R.H. Byrd, P. Lu, J. Nocedal, C. Zhu, A limited memory algorithm for bound constrained optimization, SIAM J. Scientific Stat. Comput. 16 (1995) 1190–1208.
[62] C. Zhu, R.H. Byrd, P. Lu, J. Nocedal, L-BFGS-B: algorithm 778: L-BFGS-B, FORTRAN routines for large scale bound constrained optimization, ACM Trans. Math. Softw. 23 (1997) 550–560.
[63] F. Birch, Finite elastic strain of cubic crystals, Phys. Rev. 71 (1947) 809.
[64] F. Birch, Finite strain isotherm and velocities for single-crystal and polycrystalline NaCl at high pressures and 300 k, J. Geophys. Res. 23 (1978) 1257.
[65] F.D. Murnaghan, The compressibility of media under extreme pressures, Proc. Nat. Acad. Sci. U.S.A. 30 (1944) 244.
[66] D.R. Gaskell, D.E. Laughlin, Introduction to the Thermodynamics of Materials, Taylor and Francis Inc, 2017.
[67] H. Brand, D.P. Dobson, L. Vocadlo, I.G. Wood, Melting curve of copper measured to 16 gpa using a multi-anvil press, High Pressure Res. 26 (2006) 185–191.
[68] H. Preston-Thomas, The international temperature scale of 1990 its-90, Metrologia 27 (1990) 3–10.
[69] J.B. MacChesney, P.M. Bridenbaugh, P.B. O'Conner, Thermal stability of indium nitride at elevated temperatures and nitrogen pressures, Mater. Res. Bull. 5 (1970) 783–791.
[70] G.R. Stewart, Measurement of low-tempertaure specific heat, Rev. Sci. Instrum. 54 (1998) 1–11.
[71] J. Wang, M. Zhao, S.F. Jin, D.D. Li, Debye temperature of wurtzite aln determined by x-ray powder diffraction, Powder Diffraction 29 (2014) 352–355.
[72] H.M. Ledbetter, E.R. Naimon, Elastic properties of metals and alloys. II. Copper, J. Phys. Chem. Ref. Data 3 (1974) 897.
[73] A.F. Wright, Elastic properties of zinc-blende and wurtzite AlN, GaN, and InN, J. Appl. Phys. 82 (1997) 2833.
[74] A.K. Giri, G.B. Mitra, Extrapolated values of lattice constants of some cubic metals at absolute zero, J. Phys. D: Appl. Phys. 18 (1985) L75–L78.
[75] H. Iwanaga, A. Kunishige, S. Takeuchi, Anisotropic thermal expansion in wurtzite-type crystals, J. Mater. Sci. 35 (2000) 2451–2454.
[76] I.S. Grigoriev, E.Z. Meilikhov, A.A. Radzig, Handbook of Physical Quantities, CRC Press, 1996.
[77] V.I. Koshchenko, Y.K. Grinberg, A.F. Demidenko, Thermodynamic properties of AlN (5–2700 K), GaP (5–1500 K) and BP (5–800 K), Inorg. Mater. 20 (1985) 1550–1553.
[78] M. Cardona, R.K. Kremer, R. Lauck, G. Siegle, J. Serrano, A.H. Romero, Heat capacity of PbS: isotope effects, Phys. Rev. B 76 (2007) 075211.
[79] P.W. Bridgman, The Physics of High Pressure, Dover Publications, 1931.
[80] R.E. Schmunk, C.S. Smith, Elastic constants of copper-nickel alloys, Acta Metall. 8 (1960) 396–401.
[81] L.E. McNeil, M. Grimsditch, R.H. French, Vibrational spectroscopy of aluminum nitride, J. Am. Ceram. Soc. 76 (1993) 1132–1136.
[82] M. Ueno, A. Onodera, O. Shimomura, K. Takemura, X-ray observation of the structural phase transition of aluminum nitride under high pressure, Phys. Rev. B 45 (1992) 10123.
[83] H. Xia, Q. Xia, A.L. Ruoff, High-pressure structure of gallium nitride: Wurtzite-to-rocksalt phase transition, Phys. Rev. B 47 (1993) 12925.